Modulation of Suspension Electrical Conductivity to Counter Fines Plugging in Trickle-Bed Reactors

Mohsen Hamidipour and Faïçal Larachi
Dept. of Chemical Engineering, Laval University, Québec, Canada G1V 0A6

DOI 10.1002/aic.12383
Published online August 16, 2010 in Wiley Online Library (wileyonlinelibrary.com).

Modulation of electrical conductivity in kaolin/kerosene suspensions was examined as a means for the attenuation of fines retention in trickle-bed reactors. The suspension stability was remarkably enhanced through ON-OFF concentration modulation of an electrolyte-based kerosene conductivity improver and resulted in an efficient bed-cleaning strategy under operating conditions. Periodic additions of the conductivity improver enabled fines and deposits to gain momentarily large and similar electrical charges undoing, or impeding, multilayer deposition. The time evolution of the two-phase pressure drop and specific deposit with/without conductivity improver was monitored, as well as the corresponding local deposition structure via electrical capacitance tomography (ECT). Electrical conductivity modulation was found to reduce the bed-specific deposit by an order of magnitude and the bed pressure drop increment by a factor 14. ECT imaging evaluated the efficacy of this modulation strategy in mitigating deposition and in preventing filtration-induced flow maldistribution. © 2010 American Institute of Chemical Engineers *AIChE J,* 57: 1829–1839, 2011
Keywords: filtration, deposition, trickle bed, capacitance tomography, hydrodynamics

Introduction

The quest for effective strategies to counter plugging with fines in trickle-bed hydrotreaters has witnessed an interest particularly in secondary upgrading of bitumen-derived fractions[1–3] to comply with the low-sulfur specifications of refined fractions.[4] Defined as solid materials passing a 325-mesh sieve and composed of silt, very fine quartz, and clay minerals,[5] fines cannot be entirely intercepted by the upstream filters and thus may, in the long run, foul the hydrorefining trickle-bed reactors.[6] Fines accumulation in trickle beds causes the pressure to rise by restricting the fluid flow paths and by reducing the bed permeability. Ultimately, the bed pressure drop becomes so high that the hydrotreaters must be shutdown to spare the integrity of the catalyst bed support.[6] This leads to catalyst bed replacement frequency shorter than the one dictated by the normal catalyst lifetime cycle. Deposition of fines must be minimized so that the reactor could operate, in the first place, in accordance with its catalyst lifetime cycle. Hence, there is a need for solutions to extend the operational life of hydrotreating reactors where deposition mitigation methods should be able to enhance detachment of deposits from the catalyst (or collector) surfaces. Two forces account for such release of fines: hydrodynamic and colloidal.[7]

Hydrodynamic detachment is a process whereby the deposits are rooted up at the passage of high-velocity flows that impart large enough drag forces. For soil and sandstone formations, a critical velocity (or shear stress) was shown to exist above which particles are released.[7] In catalytic reactors where loss in reactor productivity is not desirable through increasing fluid velocity, shock waves induced by

Correspondence concerning this article should be addressed to F. Larachi at faical.larachi@gch.ulaval.ca.

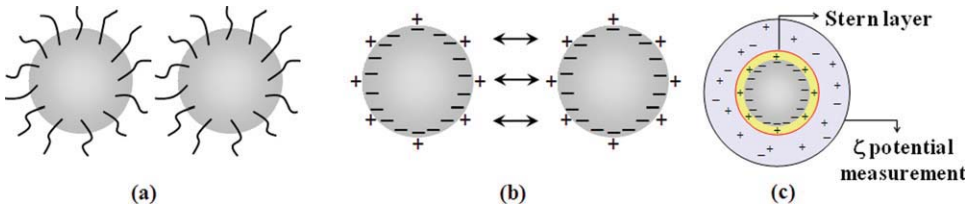

Figure 1. Suspension stability through (a) steric repulsions due to attached (macro)-molecular entities, (b) surface-charge mutual repulsions, and (c) double-layer structure.

[Color figure can be viewed in the online issue, which is available at wileyonlinelibrary.com.]

periodic velocity changes to remove fines are a better option.[8] The effect of periodic flow perturbations on the extent of filtration was experimentally investigated where the velocity of suspension and/or gas can be switched back and forth between specified levels.[9] Among the tested approaches, gas/liquid alternating cyclic operation gave the best results in terms of deposition removal.

Colloidal forces are of two types[7]: (i) the London/van der Waals attractive forces arising from the instantaneous dipole moments generated by temporary asymmetrical distribution of electrons and (ii) the electrical double-layer repulsive forces stemming from charges present on the surface of particles. These forces manifest at the approach between particles, the net balance of which dictates whether they will get attracted or repelled. Prevalence of strong repulsions, via steric repulsion and surface-charge repulsion, averts flocculation and gives rise to stable suspensions,[10] which will unlikely induce deposition in the bed.

Steric repulsion (Figure 1a) by coating kaolin particles with asphaltenes was attempted by Wang et al.[1] to prevent flocculation and reduce plugging in hydrotreating conditions. The prevailing temperature and H_2 and the water produced from hydrodeoxygenation led to removal of asphaltenes from the fines, which led back to unstable suspensions resuming deposition.[2] Similar surface treatment to prevent flocculation was tested for particles treated with humic materials to lower deposition in aqueous-media depth filtration.[11]

In surface-charge repulsion (Figure 1b), the fine is encapsulated in an electrical double layer formed by the surface charge layer on the particle screened by a diffuse layer of counterions moving close by the surface from the liquid side (Figure 1c). The zeta potential, measured in the diffuse layer between surface-attached fluid and a remote point in the fluid, gives an indication on suspension stability. For particles owning large negative or positive zeta potential, double-layer repulsions outweigh the London/van der Waals attractive forces resulting in stable suspensions.

This concept is very important wherever suspension-related topics are dealt with. For example, the critical flocculation concentration was found to be an indicator of suspension stability.[12–14] It sets the minimum concentration of counterions, which can cause instability, and represents the threshold concentration between fast and slow flocculation. With further addition of counterions, the isoelectric point will be reached where the zeta potential reduces to zero. This marks the passage between positive and negative surface charges where the suspension stability is the least.[15]

Release of subsurface fine particles is known to cause problems through either reduction of sandstone permeability due to pore clogging or migration of contaminants showing high affinity for the fines.[16,17] Through replacing groundwater with freshwater, a critical salt concentration can be reached below which the zeta potential of fines moves to the stable range and particle release becomes possible by empowering repulsion over binding among particles. For the sake of preserving sufficient porous media permeabilities, salt concentration of subground water is usually monitored so as to avoid its reduction below a critical value.

Granular filters are widely used in water and wastewater treatment to promote the removal of fines from water effluents.[18,19] Fines carrying less charges are more prone to deposition in the bed so that usually pretreatments through addition of chemicals are sought to minimize double-layer repulsive forces. The zeta potential modification is designed to destabilize the particles so as to enhance the filtration efficiency.

Apart from above aqueous media system examples, occurrence of permanent surface charges on particles in organic suspensions was known for decades.[20,21] Bed depth filtration of carbon black particles from hydrocarbon suspensions betides because collectors and fines bear opposing charges favoring mutual attractions.[22] As soon as the bed charge is neutralized due to deposition, filtration efficiency drops, which is rationalized as a setup of repulsive forces between the nascent deposit and the incoming carbon black fines. High initial filter efficiency due to attractive forces between the pristine collectors and the fine particles has been reported for kaolin/kerosene suspensions in trickle beds.[23] Multilayer layer deposition was observed to take place afterward, which was ascribed to weakly charged fines (i.e., low zeta potential) prone to bind to the developing deposits as a result of prevalence of the London/van der Waals attractive forces.

Filtration in hydrotreating trickle-bed reactors is usually viewed as a parasitic phenomenon that should be prevented to maximize catalyst usage and lifetime. As the nonpolar hydrocarbons, in play, are very weak solvents for dissolution through ionization, changes of fine–fine and/or fine–collector forces through addition of chemicals is not obvious. Therefore, enhancement of polarity of liquid hydrocarbons and studying its effect on surface charge buildup of fine particles is a worth addressing challenge.

Accumulation of electrostatic charges during handling of nonpolar hydrocarbon fuels is a well-known phenomenon. It occurs when charges are not dissipated as quickly as they form; the buildup of which depends on the hydrocarbon electrical conductivity. To prevent charge buildup, fuel electrical conductivity can be enhanced to some extent by means of electrical conductivity improvers (ECIs). The use of ECI

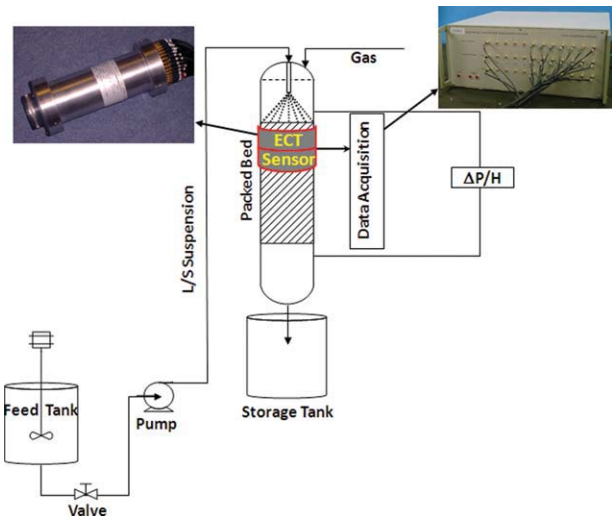

Figure 2. Schematic diagram of the experimental setup.

[Color figure can be viewed in the online issue, which is available at wileyonlinelibrary.com.]

to avert bed plugging by a control of zeta potential and stabilization of colloidal fines has never been attempted in the petroleum-refining area. In this study, we have investigated its influence on the extent of kaolin deposition in bed via electrical conductivity modulation strategy whereby brief impulsions of ECI are fed according to ON-OFF cyclic mode.

Experimental

Filtration experiments were performed in cocurrent downflow with an air/(kaolin–kerosene) suspension system in a 5.7-cm-ID Plexiglas column packed with 2.7-mm γ-alumina spheres filled up to 80-cm height. To ensure finely dispersed kaolin particles in the feed suspension, presonicated kaolin slurries were prepared and added to clean kerosene. Unless otherwise stated, the kaolin concentration in the feed suspension was 1 g/L. The experimental setup is schematically represented in Figure 2. The suspension was continuously stirred in a feed tank, pumped to the column top, and delivered through a spray nozzle. The nozzle elevation was adjusted such that the feed suspension could shower the entire cross-section at the bed top. Air was fed through several small apertures upstream of the nozzle and arranged axisymmetrically to ensure as uniform as possible gas flow distribution. Prior to filtration tests, the bed was soaked overnight in clean kerosene to make sure that the catalyst bed was fully wet.

Table 1. Approximate Chemical Composition of Electrical Conductivity Improver

Composition	Weight percent (%)	CAS No.
Toluene	10–20	108-88-3
Dodecylbenzene sulfonic acid	2–8	27176-87-0
Kerosene	60–70	8008-20-6
Solvent naphtha	2–7	64742-94-5
Polysulfone	2–7	Proprietary
Amine polymer	2–8	Proprietary

The approximate chemical composition of the ECI as disclosed by Dorf Ketal LLC is given in Table 1. To ensure that the injected additive will follow the same paths as kerosene, ECI/kerosene solutions were prepared matching as closely as possible to kerosene properties (Table 2). Zeta potential and particle size in suspensions were measured off-line using a (nano-ZS) Malvern zetasizer instrument.

Bed pressure drops were measured on-line with air-filled sampling lines by linking the discharge area below the bed and the gas load section just before the nozzle to a differential pressure transmitter. This did not require corrections of pressure measurements from uncontrolled levels of suspension in, or partial fill-up of, the connection tubes between reactor walls and pressure sensor.

Fines trapping in the bed was monitored by measuring the instantaneous overall specific deposit, $\sigma(t)$. The latter expresses the total mass of kaolin cumulatively trapped per unit reactor volume between $t = 0$ and a given instant, t. In ECI-free filtration, detachment and entrainment were rare so that the suspension inlet and outlet concentrations could be estimated using a turbidimeter calibrated for the range of experiments. As a result, $\sigma(t)$ was obtained from a mass balance around the bed using the turbidity–concentration calibration curves. Addition of ECI resulted in rapid and irregular bursts of fines in effluent concentrations due to detachment/entrainment. This invalidated reliance on exit flow sampling for mass balance estimation of specific deposit. Alternatively, the kaolin content of effluent suspension was collected integrally over a series of very fine paper filters placed at the bed exit to quantify the specific deposit every 2 h.

A 2 $\times$ 12-electrode twin-plane electrical capacitance tomography (ECT) sensor (PTL300E with DAM200E sensor controller; Process Tomography) with axial sliding capability was used for monitoring on-line and noninvasively the instantaneous evolution of the local structure of deposition as well as for substantiating the qualitative flow dynamics. The tomograph was mounted on a sleeve to slide over the column's outer diameter for interrogation of any axial region of the reactor. The twin-plane configuration allowed tomographic images to be acquired simultaneously at two axial positions by the 2 $\times$ 12 active electrodes at 50 tomographic scans per second. The Tikhonov image reconstruction algorithm was found to successfully predict the quantitative (shape) and qualitative (size) features of phantoms.[24] Therefore, the same algorithm was applied in this study.

In principle, to make ECT measurements quantitative, the sensor should be calibrated using two reference points as upper and lower limits (i.e., 0 and 100%). For filtration experiments, the aim would be to evaluate the evolving solids holdup in the bed due to fines deposition. Hence, clean (i.e., no fines) two-phase flow should be used as a zero percent calibration reference with average permittivity:

Table 2. Comparison Between Physical Properties of Kerosene and Diluted ECI (SR 1795) in Kerosene

Property	Kerosene	Diluted ECI
Density (kg/m^3)	789	798
Viscosity (mPa s)	1.1	1.1
Surface tension (mN/m)	25.3	25.3

$$E_1 = (1-\varepsilon)\cdot \bar{e}_s + \varepsilon_L \cdot e_L + (\varepsilon - \varepsilon_L)\cdot e_G \quad (1)$$

At the other extreme, uniformly saturating the initial (clean) bed porosity with kaolin deposit would contribute with an average permittivity corresponding to the 100% calibration reference:

$$E_2 = (1-\varepsilon)\cdot \bar{e}_s + \varepsilon \cdot \bar{e}_f \quad (2)$$

The intermediate instances represented by the two-phase suspension flow would then correspond to an average permittivity:

$$E_{GLf} = (1-\varepsilon)\cdot \bar{e}_s + \varepsilon_L^{\text{deposition}} \cdot e_L + \varepsilon_f \cdot \bar{e}_f + \left(\varepsilon - \varepsilon_L^{\text{deposition}} \cdot \varepsilon_f\right)\cdot e_G \quad (3)$$

A normalized permittivity, NP, could be estimated on the basis of measured permittivity for the clean two-phase flow (E_1) and a bed saturated with fines deposit (E_2) and of the measured permittivity under filtration conditions (E_{GLf}):

$$NP = \frac{E_{GLf} - E_1}{E_2 - E_1} \quad (4)$$

In these equations, $\bar{e}_s$, $\bar{e}_f$, e_L, e_G are the alumina + intraparticle kerosene effective permittivity, the deposit + intraporosity kerosene effective permittivity, the liquid and gas permittivities, respectively; and ε, ε_L, ε_G, ε_f are the bed (external) porosity, the external liquid holdup, the gas and the fines holdup, respectively, whereas the superscript "deposition" tags the liquid holdup under filtration conditions.

The main difficulty in applying the above calibration procedure dwells in setting a representative 100% reference point. Filling uniformly the available bed porosity with representative kaolin deposits having specific deposit porosity bound by the operating conditions and a priori unknown is virtually impossible to realize experimentally. Moreover, the external liquid holdup under filtration conditions and the effective permittivity of deposition + intraporosity are also unknown parameters. Involvement of such several phases in filtration experiments deprives ECT from being a quantitative tool. Hence, in this work, we contented in using it to monitor qualitatively the dynamic structure of deposition inside the bed. Thus, for commodity, the normalized permittivities were expressed using the flooded bed with kerosene as a 100% calibration point:

$$E_2 = (1-\varepsilon)\cdot \bar{e}_s + \varepsilon \cdot e_L \quad (5)$$

Witness test (reconstruction of a phantom object under filtration) proved that the measured capacitances and normalized mixture permittivity distributions reconstructed thereof can be resolved with an estimated pixel resolution of ca. 3 mm over the column cross-section.[25] Moreover, the qualitative information unveiled about the structure of deposition under two-phase flow filtration conditions proved extremely rich and useful.[25]

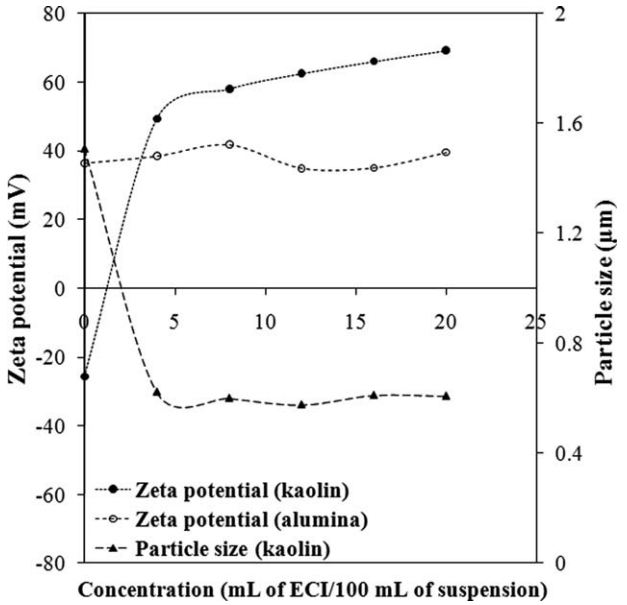

Figure 3. Kaolin and alumina zeta potential and average particle size of kaolin particles in kerosene suspensions as a function of ECI concentration in % v/v.

Results and Discussion

Effect of ECI on zeta potential and kaolin particle size

Kaolin occurs in the form of alternating bilayers of tetrahedral silicate sheets spreading along octahedral aluminate sheets.[26] The aluminate-sheet hydroxyl groups allow interbilayer van der Waals interactions between the octahedral sheet of one bilayer and the tetrahedral sheet of a nearby bilayer, which enable kaolin to stack as planar lamellas. These interactions play a role in determining the sizes and surface charges acquired by the kaolin fines present in liquid suspensions.

Even though zeta potential measurements have been already applied to nonaqueous suspensions, theoretical aspects such as the origin of surface charges and the structure of surface double layer are not well established with respect to aqueous media.[27] Consequently, interpretations of the observed phenomena in pure organic media based on those inferred from aqueous-related theories would be somehow speculative. In the context of this work, by virtue of the shift from nonpolar toward polar liquid via addition of ECI, the latter is believed to draw our nonaqueous medium nearer to aqueous media. Therefore, the arguments and discussions borrowed from the aqueous-related theories will be used to interpret our observations. To identify the effect of ECI addition on the bed–suspension interactions, zeta potential (zp) as a function of volume fraction of ECI added to the suspension is shown in Figure 3 for kaolin particles and for powdered alumina (after sieving some ground packing elements). Additionally, the average particle size of kaolin measured as a function of ECI volume fraction is shown on the same figure. The concentration of kaolin was kept at 0.1 g/L and ECI fraction was increased by increments of ca. 4 mL up to 20 mL per 100 mL of suspension.

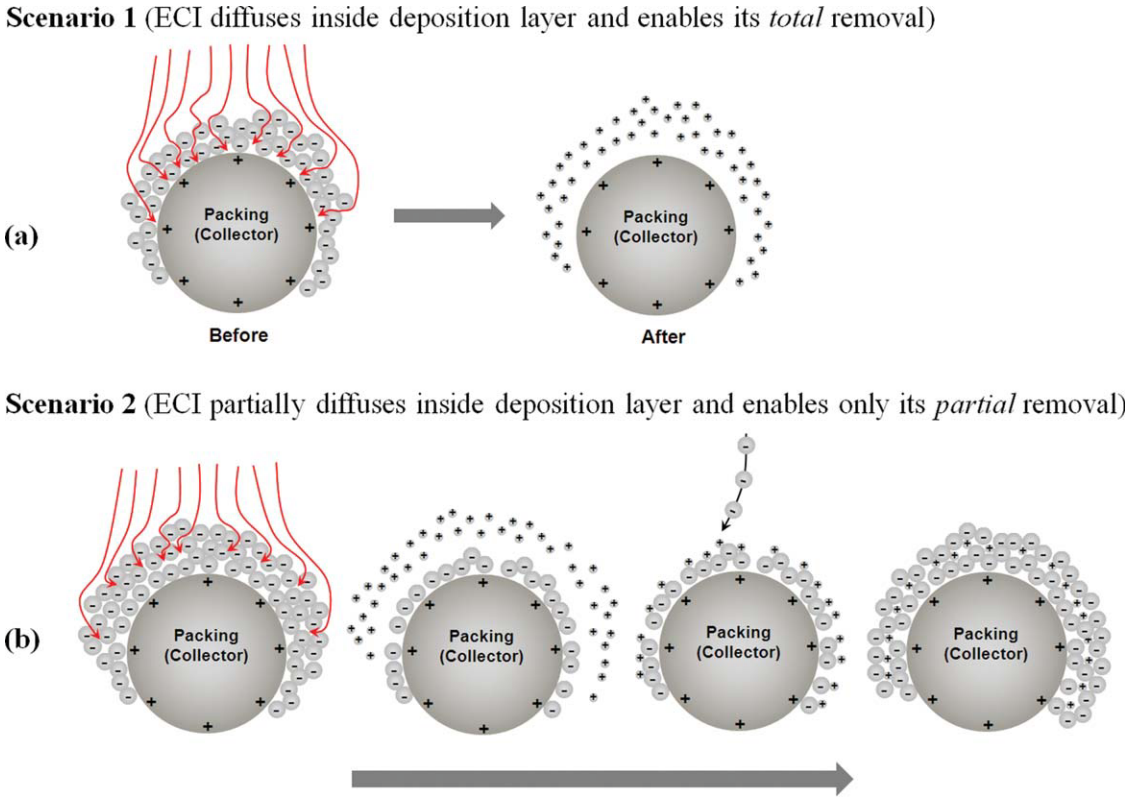

Figure 4. Schematics of the extent of ECI intrusion inside deposits and detachment/resuspension as a stable suspension.

[Color figure can be viewed in the online issue, which is available at wileyonlinelibrary.com.]

No change in electrical conductivity was observed after kaolin addition to kerosene. This would suggest that dissociation of surface groups is not an important charge-gaining mechanism.[27] Figure 3 shows that kaolin fines carry negative charges in ECI-free kerosene suspension. Their low zp value ~ -25 mV corresponds to the range of unstable suspensions. This is similar to the behavior of kaolin in aqueous media for which negative zp was reported over a wide pH range.[26] This behavior of surfaces gaining negative charges is coherent with the presence of surface groups acting as Lewis acids with respect to the liquid medium.[27] As pointed out by Miller,[26] the qualitatively close kaolin and silica electrokinetic behaviors in aqueous suspensions lean toward little influence of kaolin aluminate sheet. Also, silica has been found to be the most acidic among oxides revealing negative zp in organic solvents.[28] Hence, it is plausible that the acidic role in kaolin/kerosene suspensions is enforced by the silicate sheet of kaolin surfaces that acquire negative charges (Figure 3). An increase in kaolin surface charges was observed on addition of ECI resulting in zp sign inversion. Furthermore, 4% v/v ECI was sufficient to turn kaolin suspension into a stable one with remarkably smaller particle sizes (Figure 3). This concentration was sufficient to give rise to double-layer repulsive forces that largely offset the London/van der Waals attractive forces. Xu et al.[27] measured the size and zeta potential of carbon black particles in several liquids (aqueous and nonaqueous media). As they have also shown, larger agglomerates exist in nonpolar liquids due to the lack of sufficient charges on the surface of particles. For polar liquids, size reduction occurs due to the manifestation of surface-repulsive forces. In our case, addition of ECI shifts the nonpolar liquid toward polar. Consequently, it is reasonable to observe kaolin fines size to depend on ECI concentration. Addition of ECI can change the surface charges and therefore the zeta potential. The measured sizes through Malvern zetasizer instrument reflect the hydrodynamic sizes of existing agglomerates in the kaolin–kerosene suspension.

Increasing the electrical conductivity of kerosene through ECI addition rapidly resulted in large positively valued zp. Such a change in electrokinetic behavior could be attributed to specific adsorption of cations onto kaolin surfaces leading to charge reversal.[15] Alumina surfaces, on the contrary, gain positive charges on contact with kerosene ($\sim +35$ mV) and thus play a basic role with respect to the liquid medium. However, no change of charge was observed in this case as ECI concentration was increased (Figure 3). This would support the fact that the electrokinetic behavior of kaolin in kerosene is not dictated by its alumina layer. By altering surface charges on kaolin fines through addition of ECI to reach sufficiently high zeta potential, strong repulsive forces are enabled between the alumina (collector) particles and fines and amidst the fines themselves as well. This would result in the inhibition of deposition of kaolin fines in the bed. We will attempt to take advantage of this aspect and check the viability of zeta potential modulation in trickle-bed filtration to mitigate the deposition of fines.

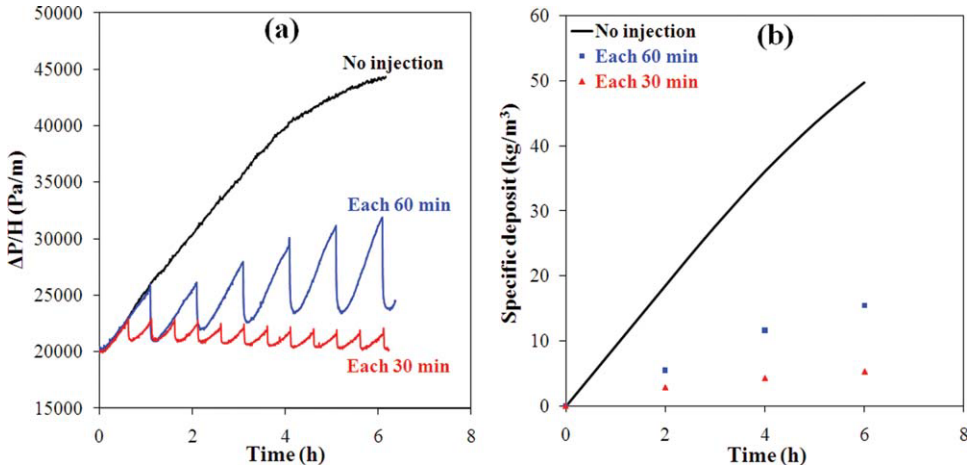

Figure 5. Time evolution of (a) two-phase pressure drop and (b) specific deposit.

Conditions: under no injection, each 60-min injection and each 30-min injection of ECI, $u_G = 0.25$ m/s, and $u_L = 0.002$ m/s. [Color figure can be viewed in the online issue, which is available at wileyonlinelibrary.com.]

ON-OFF cyclic modulation of ECI in trickle-bed filtration

The tests just discussed indicate that premixing ECI could be efficient to stabilize kaolin suspension in the colloidal range and, owing to charge reversal, to prevent deposition in the alumina bed. At the expense of forbearance of some deposition and for practical reasons, ON-OFF modulation of ECI concentration seems expedient to reduce consumption and to prevent reactor performance setbacks. Hence, removal of the deposit after being formed is worth assessing in terms of ECI efficacy to promote detachment and resuspension.

As the deposit layer is porous,[29] ECI diffusion, as sketched in Figure 4, is expected to facilitate detachment in the first place. However, upholding large positive zeta potentials for a while is anticipated to avert subsequent redepositions downstream along the reactor. Two scenarios are plausible.

- Scenario 1: ECI impulsions access the entire layers prompting surface charge changes everywhere (Figure 4a). As alumina bed charges remain unaltered, repulsive forces between surfaces charged alike will prompt, on a periodical basis, complete removal of the deposits.
- Scenario 2: Severe deposition occurs around the collectors allowing limited penetration of ECI impulsions into the deposits (Figure 4b). Only the deposit upper layers in contact with ECI will undergo detachment except some positively charged fines remaining associated at the top of the surviving deposition layer. At resumption of ECI-free suspension flow, the positively charged collector surfaces will be viewed by incoming negatively charged kaolin fines. Hence, self-accelerating multilayer deposition would set in by more positively charged kaolin fines standing by for further trapping due to increased specific surface area of deposits.

It was observed that large superficial gas velocities significantly increase bed capture efficiency through compression of the deposits.[23] This may thwart accessibility of the diffusing ECI to the whole deposit layers (Scenario 2), and hence potentially reducing detachment and resuspension. Therefore, a high gas velocity was chosen to test the bed-cleaning performance for the worst-case filtration scenario ($u_G = 0.25$ m/s, $u_L = 0.002$ m/s).

Figures 5a,b illustrate the time evolution of pressure drop and bed-specific deposit in the course of filtration without and with ECI addition. In the latter case, the experiments were performed in ECI ON-OFF mode with unsymmetrical splits where every 60 or 30 min (ECI-OFF), the kaolin/kerosene suspension flow was substituted during 10 s by an equal flow rate of fines-free ECI/kerosene solution (ECI-ON). The ON portion (or split ratio) was very small, 0.28% [$= 10/(10 + 60 \times 60)$] and 0.54% [$= 10/(10 + 60 \times 30)$] of the total periods.

Before ECI first addition, the 60-min or 30-min pressure drop portions were coincident with the no-injection curve where pressure drop and specific deposit increased monotonically (Figures 5a,b).

On ECI injection, rapid resuspensions occurred resulting in an abruptly decreasing pressure drop (Figure 5a). However, the saw-toothed shapes in Figure 5a indicate that subsequent to each ECI elution, the specific deposit and pressure drop started rising straight away. Moreover, in the long run, both exhibited a climbing trend in the case of the 10 s/60 min ON-OFF run (Figures 5a,b). This can be ascribed to gradually more limited access of ECI to some deposits in addition to induced self-accelerated capture (Scenario 2). Because either the period (60 min) is too long or the split ratio (0.28%) is too small, the deposition layers cannot be wiped off entirely. This indeed is confirmed in the 10 s/30 min ON-OFF run (Figures 5a,b) where much lower pressure drop and specific deposit were attained, approaching Scenario 1 virtually all over the bed.

ECT imaging of deposition morphology dynamics in ON-OFF modulation

As mentioned, unlike in conventional tomography applications, up to five components may be embedded in the total electrical permittivity measured by ECT in our context: the γ-alumina bed ($e_s = 4.5e_0$), the kaolin fines ($e_f = 5.0e_0$), liquid kerosene ($e_L = 2.2e_0$), air ($e_G \approx e_0$), and ECI/kerosene solution ($e^* > e_L$, not measured), where $e_0 = 8.8524 \times 10^{-12}$ F/m is the absolute vacuum permittivity.

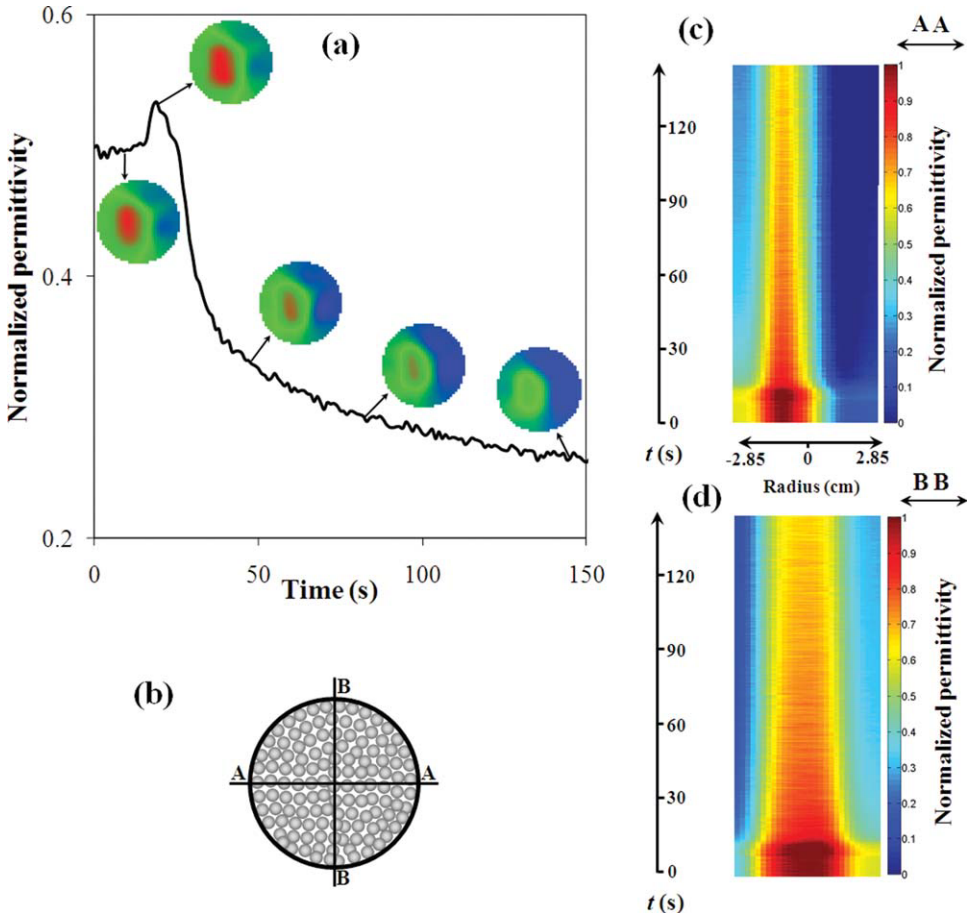

Figure 6. (a) Time variation of cross-sectionally averaged normalized permittivity during ECI fourth injection (10 s/60 min ON-OFF modulation), (b) bed cross-section view, and corresponding normalized permittivity temporal plots for (c) A-A line and (d) B-B line, H = 10 cm.

[Color figure can be viewed in the online issue, which is available at wileyonlinelibrary.com.]

ECT will definitely not lend itself to quantitative measurements. However, it turns out to be particularly powerful in sensing the tiny relative changes during deposition or entrainment of the highly contrasting kaolin phase (after prior subtraction of the invariant alumina + intraparticle kerosene bed contribution).

During the injection of ECI, the NP (Eq. 4) was computed on the basis of the measured permittivity for the clean two-phase flow (E_1, Eq. 1) and flooded bed (E_2, Eq. 5) using the measured permittivity under filtration with ECI (E^*_{GLf}) present in the stream:

$$E^*_{\mathrm{GLf}} = (1-\varepsilon)\cdot \bar{e}_{\mathrm{s}} + \varepsilon^*_{\mathrm{L}}\cdot e^* + \varepsilon^*_{\mathrm{f}}\cdot \bar{e}_{\mathrm{f}} + \left(\varepsilon - \varepsilon^*_{\mathrm{L}} - \varepsilon^*_{\mathrm{f}}\right)\cdot e_{\mathrm{G}} \quad (6)$$

where the asterisk denotes the holdup values in the presence of ECI.

Changes in time of the deposition morphology as influenced by ECI injection were assessed in terms of normalized electrical permittivity via ECT at a bed elevation H = 10 cm (upper segment of bed where deposition is most active) for the 10 s/60 min ON-OFF run (Figure 6). The selected observational time window, nearing twice the bed elution time of ECI, was zoomed in the region of the fourth pressure

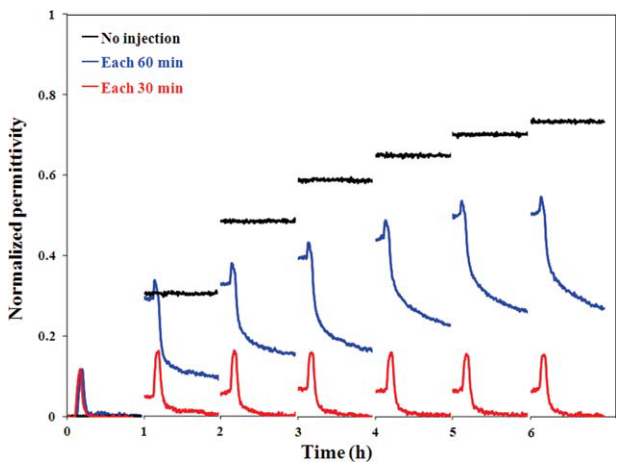

Figure 7. Time evolution of cross-sectionally averaged normalized permittivity under no injection, each 60-min injection and each 30-min injection of ECI, u_{G} = 0.25 m/s, u_{L} = 0.002 m/s, and H = 10 cm.

[Color figure can be viewed in the online issue, which is available at wileyonlinelibrary.com.]

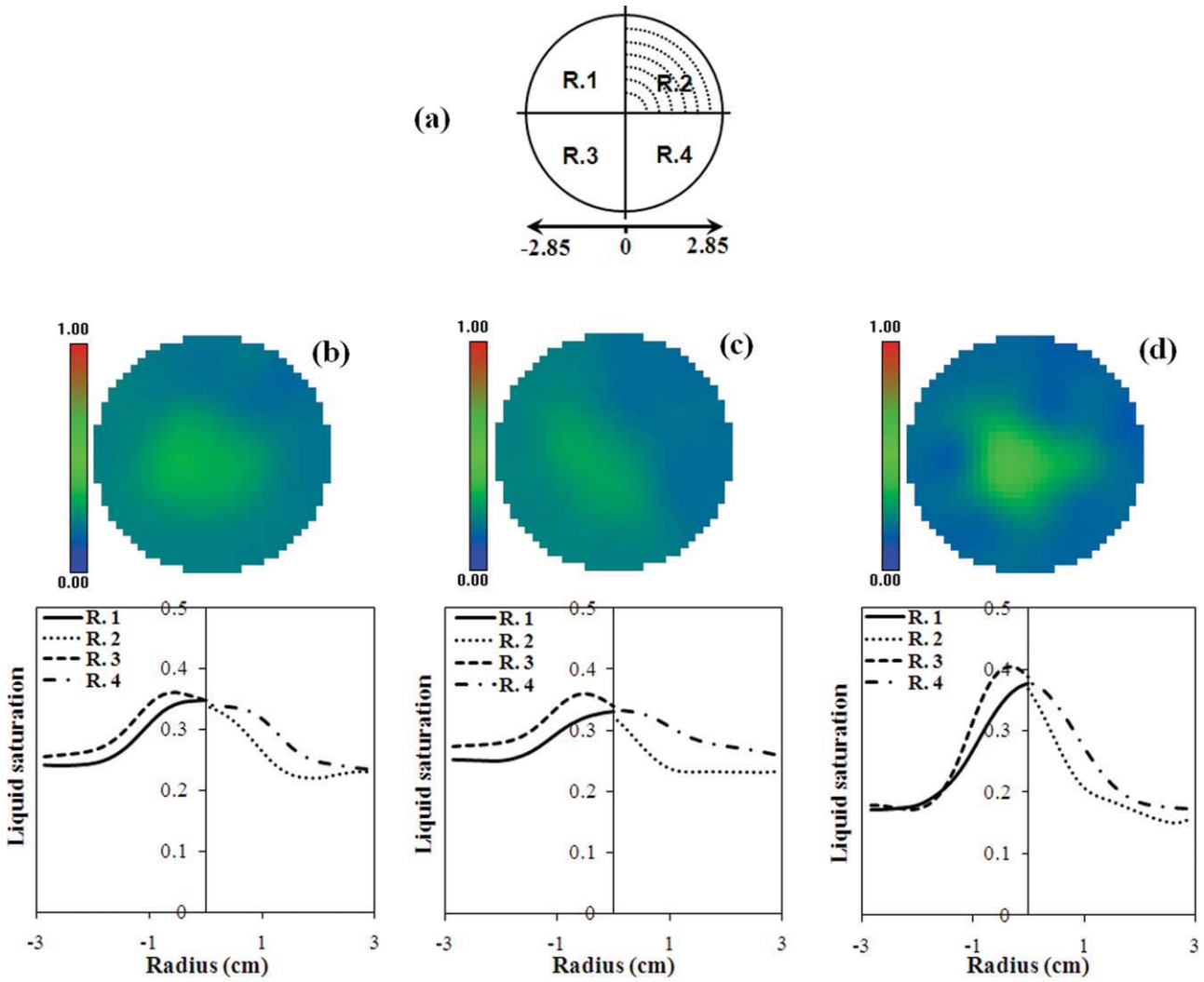

Figure 8. (a) Top view of bed cross-section divided in four regions. (b, c, and d) ECT-normalized permittivity images of liquid pattern and radial liquid distribution corresponding to different regions.

Differences are due to slight changes in bed configuration and possibly the stochastic nature of trickle flow regime, $H = 10$ cm. [Color figure can be viewed in the online issue, which is available at wileyonlinelibrary.com.]

drop peak (Figure 5a). The cross-sectionally averaged NP exhibited a peak at the passage of ECI solution ($e^* > e_L$; Figure 6a). If no detachment had occurred, NP would have retrieved, after a while, the original baseline it had prior to ECI injection. This was contradicted by the decreasing trend revealing that some detachment had taken place. Snapshots of transverse NP distributions in Figure 6a confirm this trend: a blue color denotes no deposition at all or complete removal of deposits and intermediate colors up to red implying areas with some degree of capture. To get a sense of the dynamic changes in the deposition morphology at the tracer passage, instantaneous NP distributions on A-A and B-B lines (Figure 6b) were plotted at 20-ms intervals for a duration nearing twice the reactor elution time of ECI (Figures 6c,d). Pixel intensities clearly evolved with time toward colder colors signifying removal of more deposits. Scenario 1 with nearly complete elimination of deposits took place especially alongside the walls (blue pixels), whereas Scenario 2 with partial removal of deposits manifested in the reactor core.

Temporal responses of the cross-sectionally averaged NP for the three conditions of Figure 5a are illustrated for time spans ca. 150 s every 1 h in Figure 7. According to Eq. 1, NP for clean two-phase flow before switching to suspension flow was zero. Any subsequent increase in permittivity is attributable either to the accumulation of kaolin or to the passage of ECI.

In the absence of ECI injection, NP gradually increases with a tendency to plateau (top stair-like curve) in accord with progressive reduction of filter efficiency as time passes by.[23] In cyclic modulation runs, right after injection of ECI first puff, NP experiences an overshoot then goes back to its original baseline after the chemical additive will have left the ECT field of view, as the bed still virtually preserved its pristine state. However, the NP never makes up for the original baseline following subsequent injections for the 10 s/60

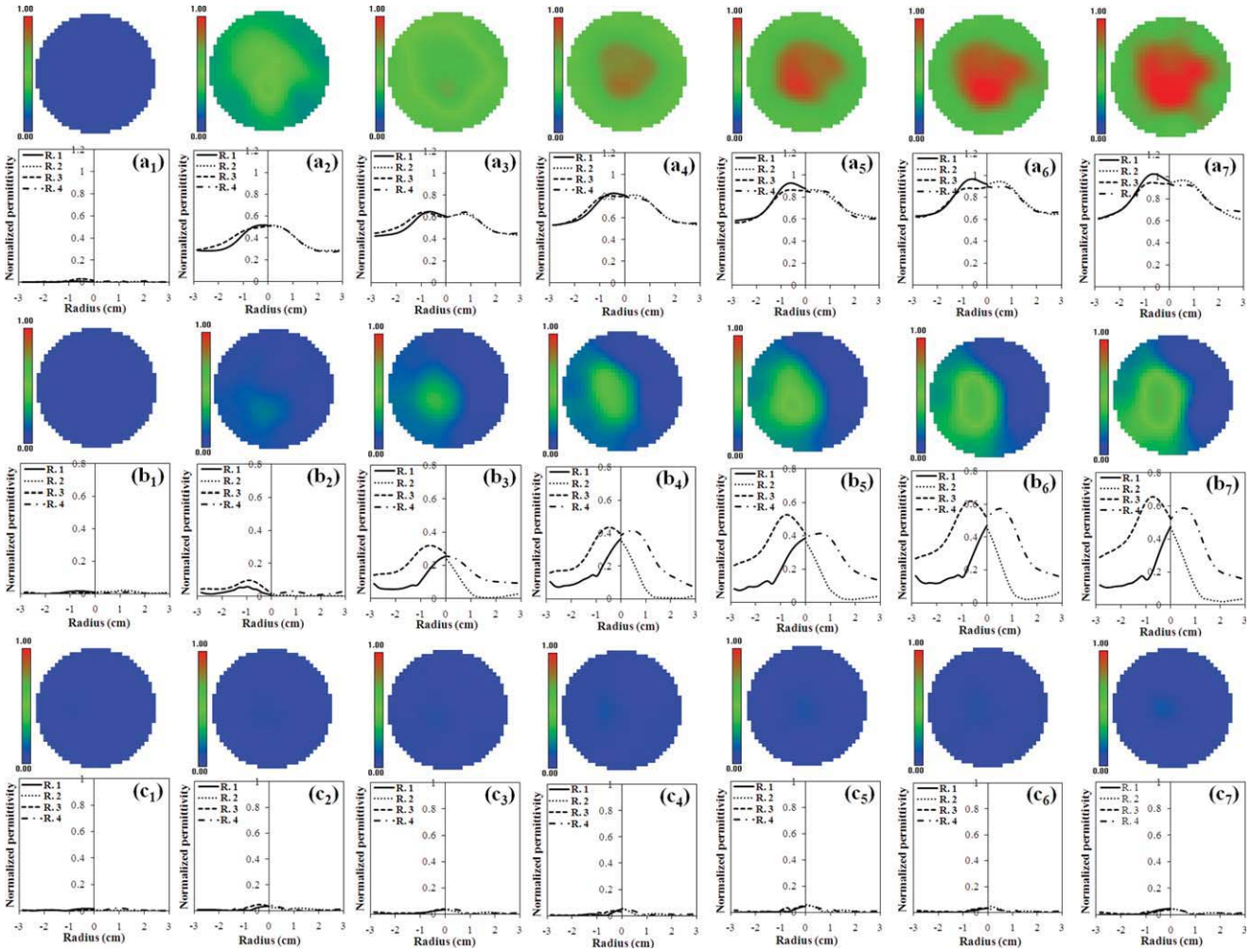

Figure 9. Two-dimensional normalized permittivity images and radial profiles of quadrant-averaged permittivities.

Quadrants R.2 = [0°–90°], R.1 = [90°–180°], R.3 = [180°–270°], R.4 = [270°–360°], time interval between each pair of images = 1 h: (a) no ECI injection, (b) ECI injection each 60 min, (c) ECI injection each 30 min, u_G = 0.25 m/s, u_L = 0.002 m/s, and H = 10 cm. [Color figure can be viewed in the online issue, which is available at wileyonlinelibrary.com.]

min ON-OFF run (Figure 7), confirming the pressure drop and specific deposit trends in Figures 5a,b. Contrariwise, fines capture is not so severe for the 10 s/30 min ON-OFF run achieving virtually complete cleansing as revealed by recovery of original baseline after elution of ECI (Figure 7). These findings suggest that a versatile cleaning method for different operating conditions would require the period and frequency of ECI injection to be carefully adjusted to maintain the bed close to its clean state.

The deposition pattern was shown to depend on the initial suspension distribution.[25] Here, the sensitivity to initial distribution is analyzed in the presence of ECI. For each experiment (i.e., each bed filling), the bed cross-section was divided into four quadrants (Figure 8a) and radial liquid distribution was measured in each quadrant using clean kerosene flow just before the switch to suspension flow (Figure 8a, Region 2). For clean conditions, the ECT sensor was calibrated between drained prewetted (as 0%) and flooded (as 100%) bed to provide liquid saturations.[25] Figures 8b–d illustrate these patterns corresponding to the previous experiments, i.e., no ECI injection, injection each 60 min, and each 30 min, respectively. For the same operating conditions, slightly different liquid patterns could arise from one bed filling to another depending on the microscopic structure of the bed and the forming flow paths. For instance, Figure 8c shows that the left quadrants (Regions 1 and 3) receive slightly more liquid, whereas Figure 8d reveals the presence of more liquid at the center. The superficial velocities of liquid and gas correspond to trickle flow regime with partial wetting. Therefore, the stochastic nature of the liquid texture (film, rivulet, drops) in forming different pathways is believed to play a role in the different distribution patterns for different bed fillings as shown in the ECT images (Figures 8b–d).

ECT images in Figures 9a1–7 show the evolution in deposition structure on an hourly basis in the absence of conductivity improver at H = 10 cm. Radial profiles of the quadrant-averaged normalized permittivities are also shown (R.1 = [90°–180°], R.2 = [0°–90°], R.3 = [180°–270°], R.4 = [270°–360°]). Because of lesser permeability in bed core, more deposition occurs there until a time-invariant structure will have developed after several hours.

ECT images corresponding to the 10 s/60 min ON-OFF run are shown in Figures 9b1–7. The images were taken right after each elution of ECI away from the ECT field of view. Most of the right side of the column cross-section turns practically clean (Scenario 1) unlike the left side which shows surviving deposits (Scenario 2). Areas receiving more suspension flow (Figure 8c) are more likely to become deposition sites. Hence, severe multilayer deposition in such regions would prevent complete wash-off of deposits thus leading to asymmetrical growths of deposits following Scenario 2. Conversely, ECT images corresponding to the 10 s/30 min ON-OFF run are shown in Figures 9c1–7. It is clearly observed that the bed remains practically clean at this depth offering much more efficient self-correction to maldistribution because of the more frequent tracer injections. The lower pressure drop and specific deposit obtained with the 10 s/30 min ON-OFF run (Figures 5a,b) and ECT local imaging confirm that cleaning trickle-bed reactors using zeta potential cyclic modulation is possible provided the proper ON-OFF cyclic modulation parameters are implemented.

Conclusion

The hydrodynamics of trickle-bed reactors was studied under two-phase flow filtration in cyclic modulation of a fuel conductivity improver. The local structure of deposition nearby the bed top where deposition is the most prominent was monitored using ECT. The following conclusions were drawn from this study:

- In organic nonpolar liquid suspensions, addition of ECIs can increase the zeta potential of solid fines. The resulting double-layer repulsive forces are strong enough to offset the London/van der Waals attractive forces yielding stable suspensions with colloidal fines.
- Injection of conductivity improver in the course of filtration was very efficient to promote detachment/entrainment of deposits following two scenarios. In the first scenario, deposition is less severe and tracer accesses all the deposits removing periodically all accumulated deposits, whereas in the second scenario, more severe deposition favors partial removal of deposits.
- Detaching deposits partially restored the higher porosity of the bed with an observed reduced pressure drop and lower bed-specific deposit.
- ECT images allowed setting the best split ratio and cyclic modulation parameters to achieve a successful zeta potential modulation for the mitigation of fines deposition in trickle-bed reactors.

Acknowledgments

The authors acknowledge the Natural Sciences and Engineering Research Council of Canada and the Natural Resources Canada for their financial support. The authors also acknowledge Dorf Ketal LLC (USA) for providing electrical conductivity improver SR 1795.

Notation

e = electrical permittivity, F/m
$\bar{e}_s$ = alumina + intraparticle kerosene effective permittivity, F/m
E = mixture permittivity, F/m
NP = normalized permittivity
u = superficial velocity, m/s
zp = zeta potential, mV

Greek letters

ε = bed porosity
ε_f = fines holdup
ε_G = gas holdup
ε_L = liquid holdup
σ = specific deposit, kg/m^3

Superscripts

* = values in the presence of ECI
1 = clean two-phase flow
2 = flooded bed

Subscripts

f = fine
G = gas
L = Liquid

Literature Citied

1. Wang S, Chung KH, Masliyah JH, Gray MR. Deposition of fine particles in packed beds at hydrotreating conditions: role of surface chemistry. *Ind Eng Chem Res*. 1999;38:4878–4888.
2. Wang S, Chung KH, Gray MR. Role of hydrotreating products in deposition of fine particles in reactors. *Fuel*. 2001;80:1079–1085.
3. Gray MR, Srinivasan N, Masliyah JH. Pressure buildup in gas–liquid flow through packed beds due to deposition of fine particles. *Can J Chem Eng*. 2002;80:346–354.
4. Sundaramurthy V, Dalai AK, Adjaye J. HDN and HDS of different gas oils derived from Athabasca bitumen over phosphorus-doped NiMo/γ-Al_2O_3 carbides. *Appl Catal B*. 2006;68:38–48.
5. Strausz OP, Lown EM. *The Chemistry of Alberta Oil Sands, Bitumens and Heavy Oils*. Calgary, AB, Canada: Alberta Energy Research Institute, 2003.
6. Koyama H, Nagai E, Torii H, Kumagaio H. Simple changes reduce catalyst deactivation, pressure-drop buildup. *Oil Gas J*. 1995;93:68–71.
7. Khilar KC, Fogler HS. *Migration of Fines in Porous Media. Theory and Applications of Transport in Porous Media*. Dordrecht: Kluwer Academic Publishing, 1998.
8. Iliuta I, Larachi F. Stretching operational life of catalytic hydrotreating trickle bed filters using liquid-induced pulsing flow. *AIChE J*. 2005;51:2034–2047.
9. Hamidipour M, Larachi F, Ring Z. Cyclic operation strategies in trickle beds and electrical capacitance tomography imaging of filtration dynamics. *Ind Eng Chem Res*. 2010;49:934–952.
10. Riddick TM. *Control of Colloid Stability Through Zeta Potential*. New York: Creative Press, 1968.
11. Amirbahman A, Olson TM. Transport of humic matter-coated hematite in packed beds. *Environ Sci Technol*. 1993;27:2807–2813.
12. Hesterberg D, Page AL. Critical coagulation concentrations of sodium and potassium illite as affected by pH. *Soil Sci Soc Am J*. 1990;54:735–739.
13. Hesterberg D, Page AL. Flocculation series test yielding time-invariant critical coagulation concentrations of sodium illite. *Soil Sci Soc Am J*. 1990;54:729–735.
14. Hsu JP, Liu BT. Effect of particle size on critical coagulation concentration. *J Colloid Interface Sci*. 1998;198:186–189.
15. Hunter RJ. *Zeta Potential in Colloid Science: Principles and Applications*. London, UK: Academic Press, 1988.
16. Khilar KC, Fogler HS. The existence of critical salt concentration for particle release. *J Colloid Interface Sci*. 1984;101:214–224.
17. Blume T, Weisbrod N, Selker JS. On the critical salt concentrations for particle detachment in homogeneous sand and heterogeneous Hanford sediments. *Geoderma*. 2005;124:121–132.
18. Kim J, Nason JA, Lawler DF. Zeta potential distributions in particle treatment processes. *J Water Supply: Res Technol AQUA*. 2006;55:461–470.

19. Kim J, Nason JA, Lawler DF. Influence of surface charge distributions and particle size distributions on particle attachment in granular media filtration. *Environ Sci Technol*. 2008;42:2557–2562.
20. Minne JL, Hermanie PHJ. Electrophoresis measurements in benzene-correlation with stability. *J Colloid Sci*. 1952;7:600–615.
21. Kitahara A, Fujii T, Katano S. Dependence of zeta potential upon particle size and capillary radius at streaming potential study in non-aqueous media. *Bull Chem Soc Jpn*. 1971;44:3242–3245.
22. Chowdiah P, Wasan DT, Gidaspow D. Electrokinetic phenomena in the filtration of colloidal suspended in non-aqueous media. *AIChE J*. 1981;27:975–984.
23. Hamidipour M, Larachi F, Ring Z. Hydrodynamic observation of trickle beds under filtration conditions. *Ind Eng Chem Res*. 2007;46:8336–8342.
24. Tibirna C, Edouard D, Fortin A, Larachi F. Usability of ECT for quantitative and qualitative characterization of trickle-bed flow dynamics subject to filtration conditions. *Chem Eng Process*. 2006;45:538–545.
25. Hamidipour M, Larachi F, Ring Z. Monitoring filtration in trickle beds using electrical capacitance tomography. *Ind Eng Chem Res*. 2009;48:1140–1153.
26. Miller JD, Nalaskowski J, Abdul B, Du H. Surface characteristics of kaolinite and other selected two layer silicate minerals. *Can J Chem Eng*. 2007;85:617–624.
27. Xu R, Wu C, Xu H. Particle size and zeta potential of carbon black in liquid media. *Carbon*. 2007;45:2806–2809.
28. Kosmulski M. Zeta potentials in nonaqueous media: how to measure and control them. *Colloids Surf A*. 1999;159:277–281.
29. Tien C, Ramarao BV. *Granular Filtration of Aerosols and Hydrosols*, 2nd ed. Great Britain: Elsevier, 2007.

Manuscript received Dec. 4, 2009, and revision received July 8, 2010.